

# Journal of Materials Chemistry A

Accepted Manuscript



This is an *Accepted Manuscript*, which has been through the Royal Society of Chemistry peer review process and has been accepted for publication.

*Accepted Manuscripts* are published online shortly after acceptance, before technical editing, formatting and proof reading. Using this free service, authors can make their results available to the community, in citable form, before we publish the edited article. We will replace this *Accepted Manuscript* with the edited and formatted *Advance Article* as soon as it is available.

You can find more information about *Accepted Manuscripts* in the [Information for Authors](#).

Please note that technical editing may introduce minor changes to the text and/or graphics, which may alter content. The journal's standard [Terms & Conditions](#) and the [Ethical guidelines](#) still apply. In no event shall the Royal Society of Chemistry be held responsible for any errors or omissions in this *Accepted Manuscript* or any consequences arising from the use of any information it contains.



Journal Name

ARTICLE

## Alkali-Modified Non-Precious Metal 3D-NiCo<sub>2</sub>O<sub>4</sub> Nanosheets for Efficient Formaldehyde Oxidation at Low Temperature

Yongchao Huang, Wenjie Fan, Bei Long, Haibo Li, Weitao Qiu, Fengyi Zhao, Yexiang Tong\*, and Hongbing Ji\*

Received 00th January 20xx,  
Accepted 00th January 20xx

DOI: 10.1039/x0xx00000x

www.rsc.org/

Cost-effective catalysts for volatile organic compounds (VOCs) oxidation are critical to energy conversion and environmental protection. Herein, we developed a new, low-cost and high-performance alkali-promoted 3D-NiCo<sub>2</sub>O<sub>4</sub> nanosheets catalysts for HCHO oxidation at room temperature. Benefiting from the large surface area, high adsorption capacity and surface hydroxyls, the alkali-promoted 3D-NiCo<sub>2</sub>O<sub>4</sub> nanosheets catalysts show substantially high catalytic activities for HCHO oxidation. The alkali-promoted 3D-NiCo<sub>2</sub>O<sub>4</sub> nanosheets yield a remarkable HCHO conversion efficiency of 95.3% at room temperature, which is not achieved by any non-precious metal based catalysts at such low temperature. Additionally, the as-prepared alkali-promoted 3D-NiCo<sub>2</sub>O<sub>4</sub> nanosheets have remained excellent catalytic performance after 200 h, which can be applied to practical application. This work provides a feasible approach to improve the efficiency of metal oxides for HCHO oxidation at low temperature.

### Introduction

Formaldehyde (HCHO) is one of the major volatile organic compounds in indoor air, which significantly impacts indoor air quality and thus influencing human health.<sup>1-4</sup> Long-term exposure to HCHO will be detrimental to human health causing headache, pneumonia, and lung cancer. Among the methods employed in the removal of HCHO, catalytic oxidation had been an outstanding approach to convert HCHO into nontoxic products such as CO<sub>2</sub> and H<sub>2</sub>O. Recently, noble metal-based catalysts (Pt, Au, Pd) had been validated to display excellent catalytic performance for HCHO oxidation at room temperature.<sup>5-9</sup> Moreover, superb catalytic activities were achieved by surface modification with alkali.<sup>10-12</sup> Zhang *et al.* demonstrated that the addition of alkali-metal ions to Pt/TiO<sub>2</sub> catalyst can significantly promote the performance of HCHO oxidation by enhancing the reaction between surface OH<sup>-</sup> and formate species at room temperature.<sup>13</sup> Nie *et al.* found that surface hydroxyls can remarkably enhance catalytic performance of Pt/TiO<sub>2</sub> toward HCHO oxidation at room temperature.<sup>14</sup> Avgouropoulos *et al.*<sup>15</sup> also revealed that alkali

promoted Pt/Al<sub>2</sub>O<sub>3</sub> catalyst for the complete oxidation of ethanol. There is a similar case that alkali obviously enhanced the catalytic performance of Ag/Co<sub>3</sub>O<sub>4</sub> for HCHO oxidation due to more surface OH<sup>-</sup> species on the catalyst surface.<sup>16</sup> However, due to the scarcity and expensive nature of noble metals, it is exceedingly desirable to remove HCHO at low temperature using noble-metal-free catalysts.

Recently, transition metal oxides especially those have large surface area and high redox property had been extensively studied as promising materials for HCHO oxidation.<sup>17, 18</sup> Bai *et al.* reported 3D-Co<sub>3</sub>O<sub>4</sub> had much higher catalytic activity for HCHO oxidation due to the large specific surface area.<sup>19</sup> Additionally, as a binary metal oxide, the spinel 3D-Mn<sub>0.75</sub>Co<sub>2.25</sub>O<sub>4</sub> possesses much higher activity because that coupling of two metal species could render the BMOs with rich redox reactions, which are beneficial to catalytic oxidation applications.<sup>20</sup> Compared with noble metal-based catalysts, the activities of transition metal oxides are not satisfied. Therefore, it is a great challenge to develop transition metal oxides catalysts with high efficiency for HCHO oxidation at low temperature.

Spinel nickel cobaltite (NiCo<sub>2</sub>O<sub>4</sub>) has been conceived as a promising cost effective and scalable alternative since it offers many advantages such as low cost, abundant resources and environmental friendliness. In its structure, the Co<sup>2+</sup> along with the Co<sup>3+</sup> at the A-sites and Ni<sup>3+</sup> along with the Ni<sup>2+</sup> at the B-sites, which provide a notable catalytic activity (Scheme 1). Herein, we address a novel alkali-promoted 3D-NiCo<sub>2</sub>O<sub>4</sub> nanosheets for the HCHO oxidation. Significantly, the catalyst

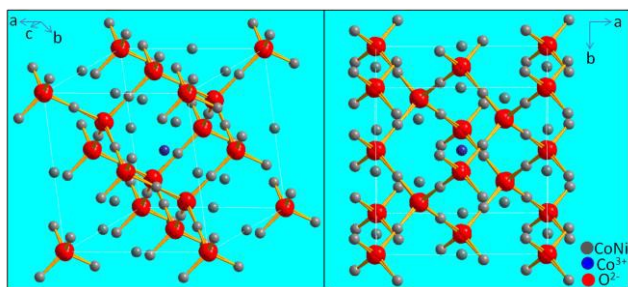
MOE of the Key Laboratory of Bioinorganic and Synthetic Chemistry, KLGEI of Environment and Energy Chemistry; The Key Lab of Low-carbon Chem & Energy Conservation of Guangdong Province, School of Chemistry and Chemical Engineering, Sun Yat-Sen University, 135 Xingang West Road, Guangzhou 510275 (P. R. China).

E-mail: jihb@mail.sysu.edu.cn (H.B.Ji)

E-mail: chedhx@mail.sysu.edu.cn (Y.X.T)

† Footnotes relating to the title and/or authors should appear here.

Electronic Supplementary Information (ESI) available: [details of any supplementary information available should be included here]. See DOI: 10.1039/x0xx00000x



**Scheme 1** Schematic unit cell structure of spinel-structured  $\text{NiCo}_2\text{O}_4$ .

could convert 95.3% of HCHO at a low temperature of 25 °C, which is not achieved by any non-precious metal based catalysts at such low temperature. The large surface area, high adsorption capacity and surface hydroxyls are suggested to greatly influence the catalytic performance of alkali-promoted 3D- $\text{NiCo}_2\text{O}_4$  nanosheets. Additionally, the surface OH<sup>-</sup> plays a main role on the reaction path of HCHO oxidation, which can directly react with formate species to produce  $\text{CO}_2$  and  $\text{H}_2\text{O}$ .

## Experimental section

### Preparation of $\text{NiCo}_2\text{O}_4$ Nanosheets

In a typical process,  $\text{Ni}(\text{NO}_3)_2 \cdot 6\text{H}_2\text{O}$  (0.3 g),  $\text{Co}(\text{NO}_3)_2 \cdot 6\text{H}_2\text{O}$  (0.6 g), and hexamethylenetetramine (0.8 g) were dissolved in an ethanol/water solution (50 mL) with a volume ratio of 3:2. After being magnetically stirred for 30 min, the as-obtained homogeneous solution was transferred into a 100 mL Teflon-lined stainless steel autoclave, sealed and maintained at 95 °C for 8 h to yield a Ni-Co precursor. Subsequently, the precursor was collected by centrifugation and washed thoroughly with water and ethyl alcohol several times and dried under 60 °C for 12 h. And then the precursor was calcined in an air atmosphere at 400 °C for 3 h with 2 °C·min<sup>-1</sup> heating rate to obtain  $\text{NiCo}_2\text{O}_4$  Nanosheets. The  $\text{NiCo}_2\text{O}_4$  Nanosheets (0.2 g) were immersed in an aqueous solution of NaOH (KOH) (100 mL) with different concentrations (0.1, 0.5, 1, 2, 4 M) at 80 °C. After stirring for 5 h, the catalysts were centrifuged and washed with water then dried under 60 °C. The resulting catalysts were denoted as  $\text{NiCo}_2\text{O}_4$ -0.1,  $\text{NiCo}_2\text{O}_4$ -0.5,  $\text{NiCo}_2\text{O}_4$ -1,  $\text{NiCo}_2\text{O}_4$ -2, and  $\text{NiCo}_2\text{O}_4$ -4, according to the concentration of NaOH.

### Characterization

X-ray diffraction (XRD) measurements were performed using a Bruker's D8 ADVANCE powder X-ray diffractometer with Cu K radiation ( $\lambda = 1.5418 \text{ \AA}$ ). Transmission electron microscopy (TEM) images were obtained with a JEM2010-HR electron microscope. Samples morphology was investigated by a field emission scanning electron microscope. Atomic force microscopy (AFM) images were obtained using a SPM-9500J3 microscopy. X-ray photoelectron spectroscopy (XPS) measurements were performed on a ESCALab250 XPS system with Al K $\alpha$  source and a charge neutralizer, and all the binding energies were referenced to the C 1s peak at 284.8 eV of the

surface adventurous carbon. Temperature-programmed reduction (TPR) analysis was conducted on a T-5080 Autochem analyzer. About 50 mg of the sample was loaded in a tube-shaped quartz cell above a small amount of quartz wool. The TPR profile of samples was recorded between 35 °C and 600 °C at a heating rate of 10 °C·min<sup>-1</sup> in 10% hydrogen in  $\text{N}_2$  with a flow rate of 50 mL·min<sup>-1</sup>. Hydrogen uptake was monitored by TCD detector. Specific surface areas (SBET) of the catalysts were calculated from a multipoint Braunauer-Emmett-Teller (BET) analysis of the nitrogen adsorption and desorption isotherms at 77 K recorded on an Autosorb-1 apparatus. The Raman spectroscopy were collected with a Laser Micro-Raman Spectrometer (Raman, Renishaw inVia). Fourier transform infrared spectra were recorded with Thermo Nicolet Nexus using the KBr disk method. In situ diffuse reflectance infrared Fourier transformed spectroscopy were measured on an EQVINOX-55 FFT spectroscope apparatus (Bruker) equipped with a diffuse reflectance accessory and a MCT detector. The sample was placed in a ceramic crucible in the chamber with  $\text{O}_2$  20 vol%, about 35% relative humidity, He balance, total flow rate of 100 mL·min<sup>-1</sup>. The thermogravimetric analysis was carried out using TA DSC Q2000 at a heating rate of 2 °C·min<sup>-1</sup> in air.

### Thermal catalytic reaction tests

The HCHO oxidation was performed in a fixed-bed reactor with 0.2 g catalyst. HCHO gas was generated and injected in an incubator (filled with a solution of 37% HCHO) kept at 0 °C, using a purified air flow ( $\text{N}_2/\text{O}_2 = 4,100 \text{ mL}\cdot\text{min}^{-1}$ ). Gas hourly space velocity (GHSV) of 60,000 mL·h<sup>-1</sup> was applied. The products of the reaction were analyzed online by an Agilent 7890A gas chromatograph with a TCD detector and a Porapak-Q column. No other carbon-containing compounds except  $\text{CO}_2$  in the products were detected for all the tested catalysts. The HCHO conversion was calculated from the  $\text{CO}_2$  content as follows:

$$\text{HCHO conversion (\%)} = [\text{CO}_2]_{\text{out}} / [\text{HCHO}]_{\text{in}} \times 100$$

$[\text{CO}_2]_{\text{out}}$  and  $[\text{HCHO}]_{\text{in}}$  in the formula are the  $\text{CO}_2$  concentration in the products and the HCHO concentration in the reactor, respectively.

## Results and discussion

### Synthesis and characterization of all the catalysts

3D- $\text{NiCo}_2\text{O}_4$  nanosheets were synthesized by a hydrothermal method and a post-calcination treatment (details in experimental section). The structural information of the samples was revealed by X-ray diffraction analysis (Fig. 1a), which verified the final sample was spinel-structured  $\text{NiCo}_2\text{O}_4$  (JCPDS 20-0781).  $\text{NiCo}_2\text{O}_4$ -X (X represent the concentration of NaOH) were obtained from the prepared  $\text{NiCo}_2\text{O}_4$  by surface modification with different concentrations of alkali. Surprisingly, the phase was not changed and no residues or contaminants had been detected, revealing the high purity of the samples (Fig. 1b). The broad diffractions peaks and the intensities are weak, which indicates the low degree of

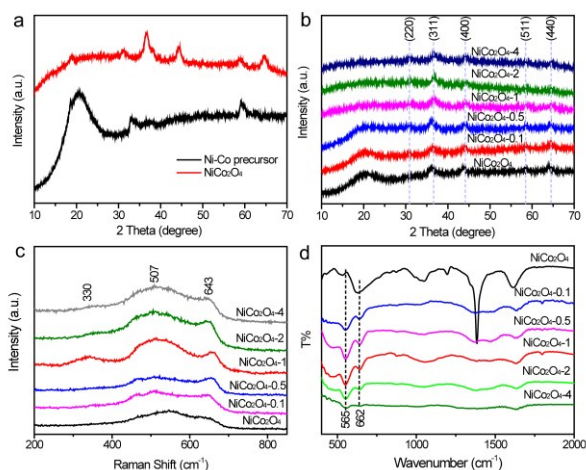


**Fig. 1** (a) XRD of the Ni-Co precursor and NiCo<sub>2</sub>O<sub>4</sub>. (b) XRD of all the samples. (c) Raman spectra and (d) FTIR spectra of all the catalysts.

crystallization and the small crystalline size of all NiCo<sub>2</sub>O<sub>4</sub> nanosheets. In order to study the detailed structural information of the samples, FTIR spectra and Raman spectroscopy were carried out. The Raman spectroscopy show three intense peaks at about 470, 550 and 643 cm<sup>-1</sup>, which are attributed to Ni-Co-O (Fig. 1c). The peaks of NiCo<sub>2</sub>O<sub>4</sub>-X show much stronger than that of NiCo<sub>2</sub>O<sub>4</sub> nanosheets, which may be the alkali can enhance the interaction between Ni-Co-O. After NaOH treatment, the peaks were shifted. This was because amount of disorder in these materials, both structural and electronic, that contributed to frequency shifts and band broadening. Additionally, a new peak at around 330 cm<sup>-1</sup> was found for NiCo<sub>2</sub>O<sub>4</sub>-1, NiCo<sub>2</sub>O<sub>4</sub>-2, NiCo<sub>2</sub>O<sub>4</sub>-4 samples, which has been assigned to the lattice mode involving mostly the displacement of oxygen atoms at octahedral sites.<sup>21-23</sup> Moreover, from FTIR spectra of catalysts, the peaks at around 662 and 565 cm<sup>-1</sup> are ascribed to the metal-oxygen vibrations of the NiCo<sub>2</sub>O<sub>4</sub> (Fig. 1d).<sup>24, 25</sup> Furthermore, the more detailed elemental composition and the oxidation state of NiCo<sub>2</sub>O<sub>4</sub> and NiCo<sub>2</sub>O<sub>4</sub>-X were further characterized by X-ray photoelectron (XPS) measurements. The surface spectra collected from the samples suggest that there are only Ni, Co, O in the catalysts, revealing the high purity of the samples. In the Ni 2p spectrum (Fig. S1b), the fitting peaks at 853.5 and 871 are indexed to Ni<sup>2+</sup>, while those at 855.5 and 873.8 are belonged to Ni<sup>3+</sup>. The Co 2p emission spectrum (Fig. S1c) was fitted with spin-orbit doublets, indexing to Co<sup>2+</sup> and Co<sup>3+</sup>. These results show that Co<sup>3+</sup>/Co<sup>2+</sup> and Ni<sup>3+</sup>/Ni<sup>2+</sup> were present in the NiCo<sub>2</sub>O<sub>4</sub> nanosheets, which is consistent with the results in the literature for NiCo<sub>2</sub>O<sub>4</sub>.<sup>26, 27</sup> Battle *et al.* found that the formula of NiCo<sub>2</sub>O<sub>4</sub> can be considered to be Co<sup>(3-δ)+</sup>[Ni<sup>(2+δ)+</sup>Co<sup>3+</sup>]<sub>2</sub>O<sub>4</sub><sup>2-</sup>, which has the redox couples Co<sup>3+</sup>/Co<sup>2+</sup> and Ni<sup>3+</sup>/Ni<sup>2+</sup> and provides a notable catalytic activity.<sup>28, 29</sup> All the aforementioned results unambiguously reveal that after surface modification with alkali the structure of NiCo<sub>2</sub>O<sub>4</sub> is preserved.

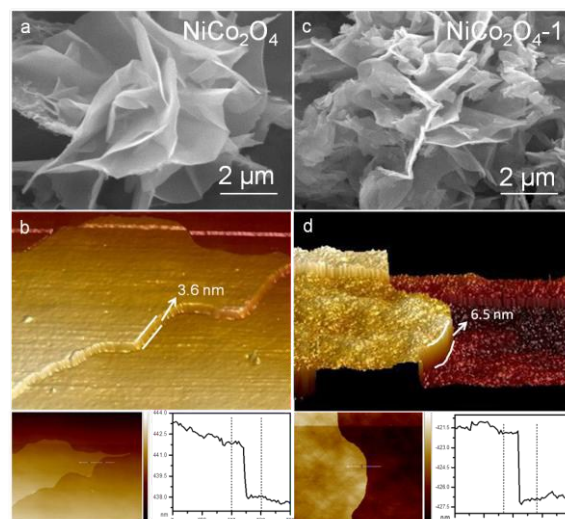


**Fig. 2** (a) SEM image and (b) AFM images of NiCo<sub>2</sub>O<sub>4</sub> nanosheets. (c) SEM image and (d) AFM images of NiCo<sub>2</sub>O<sub>4</sub>-1 nanosheets

The morphology of the catalysts was studied by scanning electron microscopy (SEM), atomic force microscopy (AFM) and transmission electron microscopy (TEM). SEM image in Fig. 2a suggests that the NiCo<sub>2</sub>O<sub>4</sub> possesses porous architectures that assembled by many nanosheets. Such porous structures afford very large active surface areas, facilitating the diffusion of guest molecules. The NiCo<sub>2</sub>O<sub>4</sub> nanosheets show folding silk-like morphology with transparent feature and the nanosheets have a thickness around 3.6 nm, indicating the ultrathin nature, as also evidenced by TEM (Fig. 2b). Surprisingly, it can be seen that the thickness of the NiCo<sub>2</sub>O<sub>4</sub>-1 nanosheets increased to 6.5 nm after the NaOH treatment. And the surface of nanosheets turns rough (Fig. 2c and d). High resolution TEM image shows high crystallinity with an interplanar spacing of 0.468 nm, which is notarized to be the d-spacing of (111) planes of NiCo<sub>2</sub>O<sub>4</sub> (Fig. 2c). The selected-area electron diffraction pattern shows well-defined diffraction rings, suggesting their polycrystalline characteristics. Significantly, an unexpected increment in thickness was found in NiCo<sub>2</sub>O<sub>4</sub>-X nanosheets, as displayed in Fig. 3b and Fig. S2. In comparison with untreated NiCo<sub>2</sub>O<sub>4</sub> nanosheets, the surface and inside of NiCo<sub>2</sub>O<sub>4</sub>-1 become disordered, which is revealed in Fig. 3d.

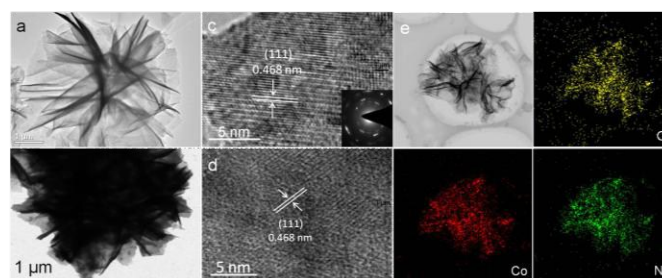


**Fig. 3** TEM images of (a) untreated NiCo<sub>2</sub>O<sub>4</sub> nanosheets and (b) NiCo<sub>2</sub>O<sub>4</sub>-1 nanosheets. HRTEM images of (c) untreated NiCo<sub>2</sub>O<sub>4</sub> nanosheets and (d) NiCo<sub>2</sub>O<sub>4</sub>-1 nanosheets. (e) EDS elemental mapping of the same region, indicating spatial distribution of Co (red), Ni (green) and O (yellow), respectively.

The results of TEM-EDS mapping of NiCo<sub>2</sub>O<sub>4</sub>-1 nanosheets reveal that the homogeneous distribution of only Ni, Co, and O in the whole selection area of porous architectures, also suggesting the high purity of the samples (Fig. 3e). Moreover, the nitrogen adsorption and desorption isotherms of catalysts are shown in Fig. S3, which belonging to IV isotherm with a hysteresis loop, indicating the presence of porous structure in the catalysts. And the pore volume is about 0.164~0.265 cm<sup>3</sup>·g<sup>-1</sup>. The results of the BET analysis reveal that the surface area of untreated NiCo<sub>2</sub>O<sub>4</sub> nanosheets (81.54 m<sup>2</sup>·g<sup>-1</sup>) is greater than that of NiCo<sub>2</sub>O<sub>4</sub>-X nanosheets (71.69~48.19 m<sup>2</sup>·g<sup>-1</sup>) (table S1).<sup>30</sup> The large surface area of NiCo<sub>2</sub>O<sub>4</sub>-X nanosheets may be one of the reasons why NiCo<sub>2</sub>O<sub>4</sub>-X nanosheets have such excellent efficiency. The higher surface area could offer more active catalytic sites for HCHO oxidation.<sup>32</sup>

#### Characterization of surface OH<sup>-</sup> on NiCo<sub>2</sub>O<sub>4</sub> nanosheets.

To provide the fingerprint evidences for probing surface OH<sup>-</sup>, the X-ray photoelectron spectroscopy (XPS) measurements were carried out, in that the presence of surface OH<sup>-</sup> causes to distinct coordinations of oxygen species. As shown in the O 1s XPS in Fig. 4a, there is one peaks at 529.5 eV in the O 1s region of NiCo<sub>2</sub>O<sub>4</sub> nanosheets, which is contributed to the typical of metal-oxygen bonds.<sup>33</sup> However, the NiCo<sub>2</sub>O<sub>4</sub>-X nanosheets appear a new peak sitting at 531 eV, which is associated with oxygen in OH<sup>-</sup>. Specifically, the intensity of 531 eV in NiCo<sub>2</sub>O<sub>4</sub>-1 nanosheets is much higher than that in other NiCo<sub>2</sub>O<sub>4</sub>-X nanosheets, indicating that the surface of the NiCo<sub>2</sub>O<sub>4</sub> catalyst is hydroxylated to some extent as a result of surface modification with alkali. Moreover, the H<sub>2</sub>-temperature-programmed reduction (TPR) measurements provided auxiliary evidence of the existence of surface OH<sup>-</sup>. Fig. 3b shows the TPR spectra of the untreated NiCo<sub>2</sub>O<sub>4</sub> and NiCo<sub>2</sub>O<sub>4</sub>-X catalysts. There are three peaks in the temperature between 100 and 500 °C. They are distinguished that corresponding to the consecutive stepwise reduction of Ni<sup>2+</sup>, Co<sup>3+</sup>, and Co<sup>2+</sup> cations, statistically distributed among tetrahedral and octahedral spinel positions. Importantly, significant enhancement in the reducibility was observed for the NiCo<sub>2</sub>O<sub>4</sub>-1 nanosheets, which have a reduction band at ca. 195 °C. It is reasonable to deduce that the peak at ca. 195 °C is due to the presence of surface OH<sup>-</sup>, leading to enhanced catalytic activity in oxidation reactions. From above discussion we believe that the OH<sup>-</sup> was bonded to the surface of NiCo<sub>2</sub>O<sub>4</sub> nanosheets rather than in form of crystal in the bulk. The absorption capabilities of HCHO gas were also exhibited to investigate the existence of surface OH<sup>-</sup> on the NiCo<sub>2</sub>O<sub>4</sub>-X nanosheets catalysts (Fig. 4c). The HCHO adsorption capability over NiCo<sub>2</sub>O<sub>4</sub> is only 9.2%, while the NiCo<sub>2</sub>O<sub>4</sub>-1 nanosheets have the largest absorption capability (15.5%) at the same condition, indicating that the surface OH<sup>-</sup> could obviously improve the adsorption capability toward HCHO. Combining with the XPS, TPR and absorption capability measurement above, we can conclude that surface OH<sup>-</sup>s are successfully introduced to the NiCo<sub>2</sub>O<sub>4</sub>-X nanosheets and the surface OH<sup>-</sup>s are believed to be the primary reason for the superior catalytic oxidation of HCHO.

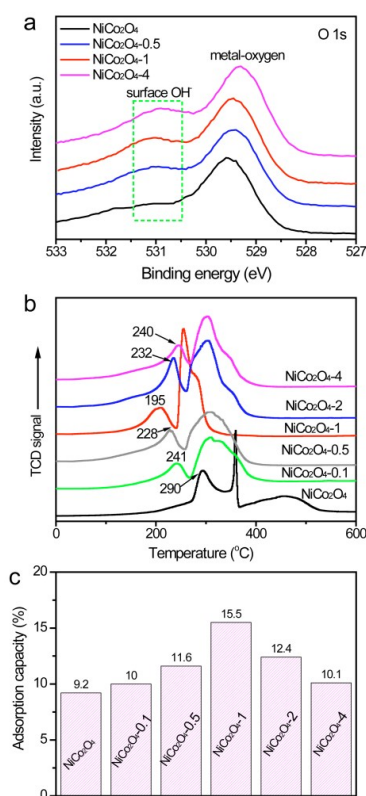


Fig. 4 (a) O1s XPS spectra of the NiCo<sub>2</sub>O<sub>4</sub> nanosheets, NiCo<sub>2</sub>O<sub>4</sub>-0.1 nanosheets, NiCo<sub>2</sub>O<sub>4</sub>-1 nanosheets and NiCo<sub>2</sub>O<sub>4</sub>-4 nanosheets. (b) H<sub>2</sub>-TPR profiles and (c) Adsorption capacity of all the samples.

#### Thermal catalytic activity of all catalysts

In order to interpret the role of surface OH<sup>-</sup> species in catalysts, the catalytic activities of HCHO oxidation on the catalysts were evaluated. Fig. 5a shows the catalytic oxidation of HCHO as a function of temperature over different catalysts. The thermal decomposition of HCHO is negligible under our experimental conditions without catalysts. Significantly, more and more HCHO is dramatically oxidized with increasing reaction temperature for all the catalysts. The untreated NiCo<sub>2</sub>O<sub>4</sub> nanosheets could convert 79% HCHO at the temperature of 100 °C, which may be because that the NiCo<sub>2</sub>O<sub>4</sub> nanosheets have large specific surface area and the high redox of Co<sup>3+</sup>/Co<sup>2+</sup> and Ni<sup>3+</sup>/Ni<sup>2+</sup>. In stark contrast, all NiCo<sub>2</sub>O<sub>4</sub>-X nanosheets catalysts display higher conversion efficiency than the pristine NiCo<sub>2</sub>O<sub>4</sub> nanosheets in the entire temperature windows, indicating that surface OH<sup>-</sup> has positive infection for HCHO oxidation. Meanwhile, it is noteworthy that NiCo<sub>2</sub>O<sub>4</sub>-1 nanosheets exhibit the remarkably higher HCHO conversion, which could convert approximately 95% of HCHO at a low temperature of 20 °C, where as the NiCo<sub>2</sub>O<sub>4</sub> nanosheets only achieve 5.2% at the same temperature. It can be summarized that such excellent performance indicates that the NiCo<sub>2</sub>O<sub>4</sub>-1 nanosheets are an outstanding active thermal catalyst at the low temperature. More importantly, to our knowledge, such superb efficiency is extensively lower than the values reported for any non-precious catalysts<sup>19, 34-39</sup> and many precious catalysts.<sup>40-42</sup> Fig. 5b compares the HCHO conversion efficiencies of our NiCo<sub>2</sub>O<sub>4</sub>-1 nanosheets with other

reported catalysts at the temperature of 20 to 100 °C with the same hourly space velocity (60,000 mL·h<sup>-1</sup>). Additionally, the quality of catalysts is a very important factor for their conversion efficiencies. Fig. 5c displays the catalytic performance with different qualities of NiCo<sub>2</sub>O<sub>4</sub>-1 nanosheets. Without doubt decreasing the quality of NiCo<sub>2</sub>O<sub>4</sub>-1 nanosheets, the efficiency declines. Noteworthy is that the amount of NiCo<sub>2</sub>O<sub>4</sub>-1 nanosheets (0.05 g) could also convert 65% HCHO, further confirming the superior performance of the NiCo<sub>2</sub>O<sub>4</sub>-1 nanosheets. Moreover, superb catalytic activities are also achieved by surface modification with KOH under the same condition, indicating that these superb catalytic activities are due to the surface OH<sup>-</sup> (Fig. S4). No other carbon-containing compounds except CO<sub>2</sub> in the products are detected for all the tested catalysts. Therefore, the above results fully indicate that the NiCo<sub>2</sub>O<sub>4</sub>-1 sample is an excellent thermal catalyst, and that surface OH<sup>-</sup> plays an important effect on the catalytic activity.

To further evaluate the stabilities of the NiCo<sub>2</sub>O<sub>4</sub> and NiCo<sub>2</sub>O<sub>4</sub>-1 nanosheets, the catalytic performances on stream at 80 °C and 25 °C for 200 h are shown in Fig. 5d, respectively. It is worth noting that the NiCo<sub>2</sub>O<sub>4</sub> nanosheets have ultrahigh stability with only 3% decrease in HCHO conversion efficiency after 200 h at 80 °C. In contrast, the NiCo<sub>2</sub>O<sub>4</sub>-1 nanosheets show much higher current decay on time than NiCo<sub>2</sub>O<sub>4</sub> catalyst. However, NiCo<sub>2</sub>O<sub>4</sub>-1 nanosheets have 84.1% of HCHO conversion efficiency after 200 h, which indicates that NiCo<sub>2</sub>O<sub>4</sub>-1 nanosheets have excellent performance and good stability. Additionally, the morphology and phase of NiCo<sub>2</sub>O<sub>4</sub>-1 nanosheets were retained after testing for 200 h (Fig. S5). In combination with the experimental results above, we can unambiguously conclude that the NiCo<sub>2</sub>O<sub>4</sub>-1 nanosheets have the outstanding performance and good stability, which holds great significance for practical applications.

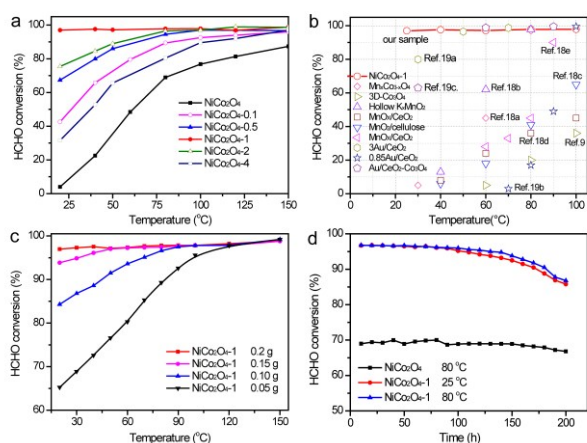


**Fig. 5** (a) HCHO conversion over different catalysts as a function of temperature (HCHO concentration = 200 ppm, 25 vol% O<sub>2</sub>, N<sub>2</sub> as balance gas, the hourly space velocity GSHV = 60,000 mL·h<sup>-1</sup>). (b) The comparison of HCHO conversion efficiencies of our NiCo<sub>2</sub>O<sub>4</sub>-1 nanosheets with the recently reported catalysts with the same GSHV. (c) HCHO conversion over NiCo<sub>2</sub>O<sub>4</sub>-1 nanosheets catalyst with different mass as a function of temperature. (d) Catalytic performance of HCHO over NiCo<sub>2</sub>O<sub>4</sub>-1 and NiCo<sub>2</sub>O<sub>4</sub> nanosheets as a function of time at 25 °C and 80 °C, respectively.

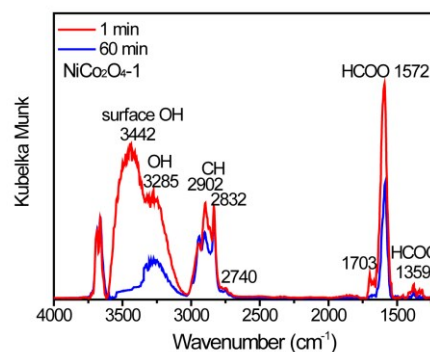


**Fig. 6** In situ DRIFTS spectra of NiCo<sub>2</sub>O<sub>4</sub>-1 nanosheets catalysts at 30 °C at 1 min and 60 min. Reaction conditions: HCHO = 200 ppm, O<sub>2</sub> 20 vol%, about 35% relative humidity, He balance, total flow rate of 100 mL·min<sup>-1</sup>.

### Reaction mechanism

The reaction mechanism of HCHO oxidation over NiCo<sub>2</sub>O<sub>4</sub>-1 nanosheets has been studied by the in-situ diffuse reflectance infrared Fourier transform (DRIFTS) experiments, which has already proved to be a powerful technology for direct visualization of the active species groups on the catalyst. In this regard, the in-situ DRIFTS spectra of NiCo<sub>2</sub>O<sub>4</sub>-1 nanosheets is shown in Fig. 6. It is seen that after exposing the sample to a flow of O<sub>2</sub>+HCHO (37%)+He at 30 °C, the peaks appeared at 1360 and 1590 cm<sup>-1</sup> belong to the symmetric stretch and asymmetric stretch of COO; 2840 and 2950 cm<sup>-1</sup> belong to the asymmetric stretch and symmetric stretch of CH of formate, respectively. Broad peaks between 3000 and 3500 cm<sup>-1</sup> can be assigned to the OH<sup>-</sup> species on the catalyst surface. After 60 min, the intensity of the OH<sup>-</sup> peak at 3442 cm<sup>-1</sup> decreased, indicating the reaction between formate and active OH<sup>-</sup> species on the NiCo<sub>2</sub>O<sub>4</sub>-1 nanosheets surface. It means that the pathway of reaction for HCHO oxidation on NiCo<sub>2</sub>O<sub>4</sub>-1 nanosheets follows the HCHO → CHOO<sup>-</sup> + OH<sup>-</sup> → CO<sub>2</sub> + H<sub>2</sub>O route, which were also demonstrated in 2% Na-1% Pt/TiO<sub>2</sub><sup>13</sup> and K-Ag/Co<sub>3</sub>O<sub>4</sub>.<sup>16</sup> Certain conclusions can be made from these studies, and the surface OH<sup>-</sup> plays a pivotal role in proving the HCHO oxidation of NiCo<sub>2</sub>O<sub>4</sub>-1 nanosheets at low temperature, which could provide guidelines for understanding the importance of the surface OH<sup>-</sup> for HCHO oxidation. From the experimental results above, the pronounced catalytic performance of NiCo<sub>2</sub>O<sub>4</sub>-1 nanosheets is attributed to a synergistic effect of the following factors. First, the 3D-NiCo<sub>2</sub>O<sub>4</sub>-1 nanosheets have a pore structure and large surface area, which are good for the HCHO to diffuse and may offer more active sites for HCHO conversion. Second, more surface OH<sup>-</sup> on the NiCo<sub>2</sub>O<sub>4</sub>-1 nanosheets enhanced the adsorption capacity of HCHO. Some results proposed that the absorption over catalysts was the crucial step for HCHO oxidation, which could make the HCHO easily react with the catalysts. Third, the high redox of NiCo<sub>2</sub>O<sub>4</sub>-1 nanosheets enhanced the performance. The activation and migration of oxygen species on catalysts are dependent on the redox cycles of Co<sup>3+</sup>/Co<sup>2+</sup> and Ni<sup>3+</sup>/Ni<sup>2+</sup>. The increase in Co<sup>3+</sup> and Ni<sup>2+</sup> can enhance the redox cycles of NiCo<sub>2</sub>O<sub>4</sub>-1 nanosheets, which is

favourable for the HCHO oxidation. Last, the surface OH<sup>-</sup> played a main role on the reaction path of HCHO oxidation, which can directly react with formate species to produce CO<sub>2</sub> and H<sub>2</sub>O. Therefore, the superb catalytic performance for the NiCo<sub>2</sub>O<sub>4</sub>-1 nanosheets can be attributed to the synergistic effects of large surface area, enhanced HCHO adsorption, the redox cycles of Co<sup>3+</sup>/Co<sup>2+</sup> and Ni<sup>3+</sup>/Ni<sup>2+</sup>, and the surface OH<sup>-</sup>.

## Conclusions

In summary, we have demonstrated a novel alkali-promoted 3D-NiCo<sub>2</sub>O<sub>4</sub> nanosheets for the HCHO oxidation. Significantly, it could convert 95.3% of HCHO into CO<sub>2</sub> and H<sub>2</sub>O at a low temperature of 25 °C, which is not achieved by any non-precious metal based catalysts at such low temperature. Benefiting from the large surface area, high adsorption capacity, and high redox, the alkali-promoted 3D-NiCo<sub>2</sub>O<sub>4</sub> nanosheets catalyst showed substantially high catalytic activity for HCHO oxidation. Additionally, the surface OH<sup>-</sup> played a main role on the reaction path of HCHO oxidation, which can directly react with formate species to produce CO<sub>2</sub> and H<sub>2</sub>O. As a consequence, the vital HCHO catalytic oxidation performance of the alkali-promoted 3D-NiCo<sub>2</sub>O<sub>4</sub> nanosheets can be anticipated to be a candidate to replace the noble metals catalysts. Furthermore, this work provides a new insight to design low-cost and high-efficiency non-precious metal based catalysts for low-temperature thermal catalytic oxidation of VOCs.

## Acknowledgements

This work was preliminarily supported by the National Science Fund for Distinguished Young Scholars (21425627), the Science and Technology Plan Project (2013B090600036), the Natural Science Foundation of China (21461162003 and 395 21425627), and Natural Science Foundation (2014KTSCX004 and 2014A030308012) of Guangdong Province, China.

## Notes and references

- J. Xu, T. White, P. Li, C. He and Y. F. Han, *J. Am. Chem. Soc.*, 2010, **132**, 13172-13173.
- Q. Yuan, Z. Wu, Y. Jin, F. Xiong and W. Huang, *J. Phys. Chem. C*, 2014, **118**, 20420-20428.
- L. Nie, J. Yu and J. Fu, *ChemCatChem*, 2014, **6**, 1983-1989.
- Q. Wang, W. Jia, B. Liu, W. Zhao, C. Li, J. Zhang and G. Xu, *Chem. – An Asian J.*, 2012, **7**, 2258-2267.
- Z. Xu, J. Yu and M. Jaroniec, *Appl. Catal. B: Environ.*, 2015, **163**, 306-312.
- Z. Yan, Z. Xu, J. Yu and M. Jaroniec, *Environ. Sci. Technol.*, 2015, **49**, 6637-6644.
- C. Zhang, H. He and K. i. Tanaka, *Catal. Commun.*, 2005, **6**, 211-214.
- H. Tan, J. Wang, S. Yu and K. Zhou, *Environ. Sci. Technol.*, 2015, **49**, 8675-8682.
- H. Huang and D. Y. Leung, *ACS Catal.*, 2011, **1**, 348-354.
- C. Zhang, Y. Li, Y. Wang and H. He, *Environ. Sci. Technol.*, 2014, **48**, 5816-5822.
- P. Zhou, J. Yu, L. Nie and M. Jaroniec, *J. Mater. Chem. A*, 2015, **3**, 10432-10438.
- J. Yu, X. Li, Z. Xu and W. Xiao, *Environ. Sci. Technol.*, 2013, **47**, 9928-9933.
- C. Zhang, F. Liu, Y. Zhai, H. Ariga, N. Yi, Y. Liu, K. Asakura, M. Flytzani - Stephanopoulos and H. He, *Angew Chem. Int. Edit.*, 2012, **51**, 9628-9632.
- L. Nie, J. Yu, X. Li, B. Cheng, G. Liu and M. Jaroniec, *Environ. Sci. Technol.*, 2013, **47**, 2777-2783.
- G. Avgouropoulos, E. Oikonomopoulos, D. Kanistras and T. Ioannides, *Appl. Catal. B: Environ.*, 2006, **65**, 62-69.
- B. Bai and J. Li, *ACS Catal.*, 2014, **4**, 2753-2762.
- Y. Huang, B. Long, M. Tang, Z. Rui, M. S. Balogun, Y. Tong and H. Ji, *Appl. Catal. B: Environ.*, 2016, **181**, 779-787.
- Z. Ren, V. Botu, S. Wang, Y. Meng, W. Song, Y. Guo, R. Ramprasad, S. L. Suib and P. X. Gao, *Angew Chem. Int. Edit.*, 2014, **53**, 7223-7227.
- B. Bai, H. Arandiyani and J. Li, *Appl. Catal. B: Environ.*, 2013, **142**, 677-683.
- Y. Wang, X. Zhu, M. Crocker, B. Chen and C. Shi, *Appl. Catal. B: Environ.*, 2014, **160**, 542-551.
- C. F. Windisch, G. J., Pacific Northwest National Laboratory (PNNL), Richland, WA (US), 2004.
- C. F. Windisch, K. F. Ferris and G. J. Exarhos, *J. Vacuum Sci. & Tech. A*, 2001, **19**, 1647-1651.
- C. F. Windisch Jr, G. J. Exarhos and S. K. Sharma, *J. Appl. Phys.*, 2002, **92**, 5572-5574.
- P. Nkeng, G. Poillierat, J. Koenig, P. Chartier, B. Lefez, J. Lopitiaux and M. Lenglet, *J. Electrochem. Soc.*, 1995, **142**, 1777-1783.
- B. Lefez, P. Nkeng, J. Lopitiaux and G. Poillierat, *Mater. Res. Bull.*, 1996, **31**, 1263-1267.
- C. Yuan, J. Li, L. Hou, X. Zhang, L. Shen and X. W. D. Lou, *Adv. Funct. Mater.*, 2012, **22**, 4592-4597.
- L. Shen, Q. Che, H. Li and X. Zhang, *Adv. Funct. Mater.*, 2014, **24**, 2630-2637.
- P. D. Battle, A. K. Cheetham and J. B. Goodenough, *Mater. Res. Bull.*, 1979, **14**, 1013-1024.
- M. Iliev, P. Silwal, B. Loukya, R. Datta, D. Kim, N. Todorov, N. Pachauri and A. Gupta, *J. Appl. Phys.*, 2013, **114**, 033514-033522.
- Q. Wang, B. Liu, X. Wang, S. Ran, L. Wang, D. Chen and G. Shen, *J. Mater. Chem.*, 2012, **22**, 21647-21653.
- B. Cui, H. Lin, J. B. Li, X. Li, J. Yang and J. Tao, *Adv. Funct. Mater.*, 2008, **18**, 1440-1447.
- L. Qi, B. Cheng, J. Yu and W. Ho, *J. Hazard. Mater.*, 2015, **15**, 522-530.
- T. Choudhury, S. Saied, J. Sullivan and A. Abbot, *J. Phys. D: Appl. Phys.*, 1989, **22**, 1185-1195.
- C. Shi, Y. Wang, A. Zhu, B. Chen and C. Au, *Catal. Commun.*, 2012, **28**, 18-22.
- H. Chen, J. He, C. Zhang and H. He, *J. Phys. Chem. C*, 2007, **111**, 18033-18038.

36. L. Zhou, J. He, J. Zhang, Z. He, Y. Hu, C. Zhang and H. He, *J. Phys. Chem. C*, 2011, **115**, 16873-16878.
37. J. Quiroz, J. M. Giraudon, A. Gervasini, C. Dujardin, C. Lancelot, M. Trentesaux and J. F. Lamonier, *ACS Catal.*, 2015, **5**, 2260-2269.
38. X. Tang, Y. Li, X. Huang, Y. Xu, H. Zhu, J. Wang and W. Shen, *Appl. Catal. B: Environ.*, 2006, **62**, 265-273.
39. Y. Huang, H. Li, M. S. Balogun, H. Yang, Y. Tong, X. Lu and H. Ji, *RSC Adv.*, 2014, **5**, 7729-7733.
40. H. F. Li, N. Zhang, P. Chen, M. F. Luo and J. Q. Lu, *Appl. Catal. B: Environ.*, 2011, **110**, 279-285.
41. Y. Shen, X. Yang, Y. Wang, Y. Zhang, H. Zhu, L. Gao and M. Jia, *Appl. Catal. B: Environ.*, 2008, **79**, 142-148.
42. B. Liu, Y. Liu, C. Li, W. Hu, P. Jing, Q. Wang and J. Zhang, *Appl. Catal. B: Environ.*, 2012, **127**, 47-58.

## Graphical Abstract

We developed a new, low-cost and high-performance alkali-promoted 3D-NiCo<sub>2</sub>O<sub>4</sub> nanosheets for efficient catalytic HCHO oxidation at low temperature.

